Nano Research 2018, 11(7): 3722–3729
https://doi.org/10.1007/s12274-017-1940-5
Research Article
ISSN 1998-0124
CN 11-5974/O4

Recovery of edge states of graphene nanoislands on an iridium substrate by silicon intercalation

Hui Chen[1], Yande Que[1], Lei Tao[1], Yu-Yang Zhang[1,2], Xiao Lin[1], Wende Xiao[1], Dongfei Wang[1], Shixuan Du[1] (✉), Sokrates T. Pantelides[2,3,1], and Hong-Jun Gao[1] (✉)

[1] *Institute of Physics & University of Chinese Academy of Sciences, Chinese Academy of Sciences, Beijing 100190, China*
[2] *Department of Physics and Astronomy, Vanderbilt University, Nashville, Tennessee 37235, USA*
[3] *Department of Electrical Engineering and Computer Science, Vanderbilt University, Nashville, Tennessee 37235, USA*

Received: 15 September 2017
Revised: 22 November 2017
Accepted: 29 November 2017

KEYWORDS
graphene nanoisland,
zigzag edge,
edge state,
scanning tunneling microscopy,
density functional theory

ABSTRACT

Finite-sized graphene sheets, such as graphene nanoislands (GNIs), are promising candidates for practical applications in graphene-based nanoelectronics. GNIs with well-defined zigzag edges are predicted to have spin-polarized edge-states similar to those of zigzag-edged graphene nanoribbons, which can achieve graphene spintronics. However, it has been reported that GNIs on metal substrates have no edge states because of interactions with the substrate. We used a combination of scanning tunneling microscopy, spectroscopy, and density functional theory calculations to demonstrate that the edge states of GNIs on an Ir substrate can be recovered by intercalating a layer of Si atoms between the GNIs and the substrate. We also found that the edge states gradually shift to the Fermi level with increasing island size. This work provides a method to investigate spin-polarized edge states in high-quality graphene nanostructures on a metal substrate.

1 Introduction

Graphene nanostructures have attracted increasing interest in recent years, as their electronic and magnetic properties can be tuned by their size, shape, and edge structure [1–3]. Graphene nanostructures with zigzag edges have edge states that are predicted to be spin-polarized [4–6]. The spin-polarized edge states can introduce a variety of intriguing physical properties, e.g., half-metallic behavior [5], spin-filtering transport properties [7], and spin confinement [8]. To date, the study of edge states has mainly focused on zigzag-edged graphene nanoribbons (ZGNRs), where two edges are parallel and long (infinite) [9, 10]. In addition to GNRs, graphene nanoislands (GNIs) with confinement in two dimensions are another fascinating graphene nanostructure owing to their potential use in both bottom-up and top-down approaches for quantum-dot technology [11, 12]. GNIs have more diversity in shape and size than GNRs. GNIs with different shapes and

Address correspondence to Shixuan Du, sxdu@iphy.ac.cn; Hong-Jun Gao, hjgao@iphy.ac.cn

sizes provide a good test bed for understanding the interactions among edge states at various finite edges [13–15], which can be useful for the design of practical graphene-based spintronics.

Although there are some theoretical reports about the edge states in GNIs [13–15], only a few experimental studies have been carried out. In experiments, atomically well-defined zigzag edges are necessary to study the edge states, as the electronic properties of the edges are sensitive to edge roughness [16]. So far, hexagonal GNIs with well-defined zigzag edges have been synthesized on Pt(111) [17], Ir(111) [18–20], and Ru(0001) [21] substrates. However, no edge states have been observed for GNIs with zigzag edges grown on these substrates. The absence of edge states is attributed to the strong interaction between the low-energy edge states of the GNIs and the nearby free electrons of the metal substrate [20]. Similar results are known for GNRs with zigzag edges, where the edge states are suppressed by the metal substrate, but are recovered when the GNRs are transferred to an insulating surface [9, 22].

Intercalation between the graphene and the metal substrates has been demonstrated to effectively decouple monolayer graphene and graphene nanostructures from the substrates [23–26]. In particular, the atomic edge structure recovers the structure of quasi-free-standing graphene edges upon intercalation of Au between graphene nanoflakes and an Ir substrate [23], but recovery of the edge states has not been reported. More recently, the frontier states of armchair GNRs on a Au substrate were recovered after Si-intercalation [24]. However, recovery and direct observation of zigzag edge states on GNIs on metal substrates such as Ru, Pt and Ir, where the edges feature the highest quality, remain an open issue.

In this paper, we report the recovery of edge states at well-defined zigzag edges of GNIs on an Ir(111) substrate by intercalating a single layer of Si atoms between the GNIs and the Ir substrate. We used low-temperature scanning tunneling microscopy and spectroscopy (LT-STM/STS) in combination with density functional theory (DFT) calculations to demonstrate the recovery of edge states that are known to exist on the zigzag edges of freestanding GNIs, but are suppressed when the GNIs are on an Ir substrate. The intercalated Si layer acts as a buffer layer to efficiently reduce the interaction between the GNIs and the Ir substrate. By measuring the edge states on the edges of GNIs of different sizes, we found that the edge states gradually shifted to the Fermi level with increasing island size due to the quantum confinement effect. This effect was confirmed by DFT calculations, which also showed that the edge states of GNIs with an irregular hexagonal shape are spin-polarized.

2 Results and discussion

Figure 1(a) shows a large-scale STM image of GNIs. All GNIs grown on Ir(111) have a uniform height of about 0.2 nm, corresponding to a single-layer thickness, and the lateral size of the GNIs varies from a few nanometers to several tens of nanometers. The surfaces of the GNIs exhibit regular moiré superstructures with a periodicity of about 2.5 nm due to the lattice mismatch between the graphene and the Ir(111) surface [27–29]. Most of the isolated GNIs have a roughly hexagonal shape and the atomic-resolution STM image in Fig. S1(a) in the Electronic Supplementary Material (ESM) clearly shows the zigzag edges of the GNIs. By measuring a series of dI/dV spectra across the zigzag edges of GNIs of different sizes (see Fig. S1 in the ESM), we confirmed that there were no edge states at the zigzag edges of GNIs on an Ir(111) substrate due to the strong interaction between the GNIs and the Ir substrate [20].

When Si atoms were initially evaporated on the sample, they preferentially covered the bare Ir(111) surface and exhibited an ordered moiré pattern with a periodicity of about 1.2 nm (Fig. 1(b)). A structure with a periodicity of about 1.2 nm was also observed at the center of the GNIs after cycles of Si evaporation and subsequent annealing completely covered the bare Ir(111) surface with the ordered moiré pattern (Fig. 1(c)). The high-resolution STM image and corresponding fast Fourier transform (FFT) patterns indicate that the ordered moiré pattern on the bare Ir(111) surface and at the center of the GNIs is a ($\sqrt{19} \times \sqrt{19}$)R23.4° superstructure with respect to the Ir(111) substrate (Fig. S2 in the ESM). The appearance of a ($\sqrt{19} \times \sqrt{19}$)R23.4° superstructure indicates that the Si has been successfully intercalated between the GNIs and Ir substrate [25]. As more Si was evaporated onto the sample, the intercalated Si layer gradually extended to the edges of the GNIs (Fig. 1(d)). STM measurements showed that the defect density of the GNIs after Si intercalation was very similar to that of the GNIs before Si intercalation, suggesting that Si intercalation has no significant

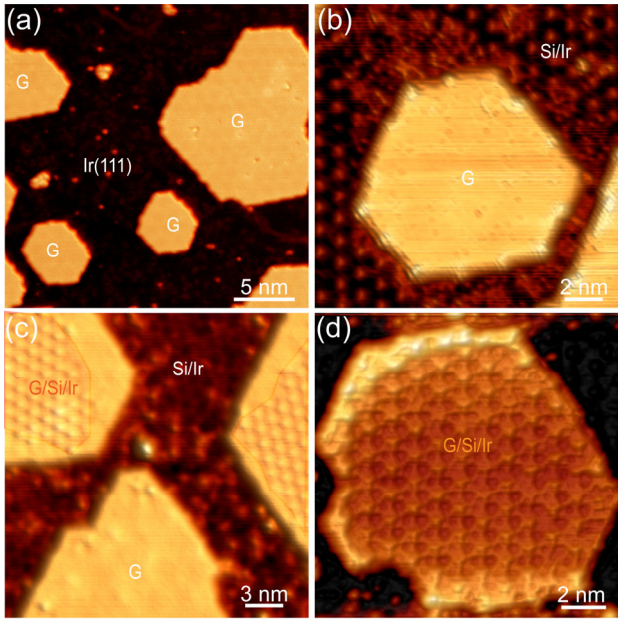

Figure 1 STM images of GNIs on Ir(111) before and after Si intercalation. (a) A large scale STM image showing the nearly hexagonal shape of as-grown GNIs with various lateral sizes (sample bias, U = –200.0 mV; tunneling current, I = 0.01 nA). (b) An STM image showing the preferential occupation of Si atoms on the bare Ir(111) surface around a hexagonal GNI during the initial phase of Si intercalation (U = –200.0 mV, I = 0.1 nA). (c) An STM image showing the intercalation of Si at the center of GNIs with increasing coverage of Si (U = –200.0 mV, I = 0.1 nA). (d) An STM image showing the formation of a complete Si layer between the GNIs and the Ir substrate (U = –200.0 mV, I = 0.1 nA).

effect on the quality of the GNIs.

It is worth mentioning that the Si intercalation starts exclusively from the center of the GNIs, rather than from the edges; therefore, Si intercalation cannot be attributed to the diffusion of Si atoms through the edges of GNIs [30]. This observation indicates that the interaction between the zigzag edges of GNIs and the Ir substrate is much stronger than that between the center of the GNIs and the Ir substrate before Si intercalation [31].

The graphene edges are terminated with H-atoms that come from the C_2H_4 molecules used during the growth procedure. As the experiments were done in ultra-high-vacuum (UHV), modification of the edges by other molecules or atoms can be excluded. The atomic structure of the GNIs before and after intercalation, together with DFT calculations, is shown in Fig. S3 in the ESM. The STM images show well-defined zigzag edges before and after Si intercalation (Figs. S3(a) and S3(b) in the ESM). The edges of GNI/Ir(111) show a bending configuration toward the Ir(111) surface due to the strong interactions between the edge and the substrate (Fig. S3(c) in the ESM). However, after Si intercalation, the edge becomes flat, indicating a much weaker coupling between the edge and the Si atoms (Fig. S3(d) in the ESM). This feature is consistent with that observed when Au was intercalated between graphene nanoflakes and an Ir substrate [23].

After the intercalation of a complete Si layer between the GNIs and the Ir substrate, we collected a series of dI/dV spectra across and along the edges of the GNIs. Figure 2(a) shows a typical STM image of a straight zigzag edge of a Si intercalated GNI. A small peak at ~ –50 mV can be seen in the dI/dV spectra of Si/Ir, which is attributed to the electronic states of Si (Fig. S4 in the ESM). The dI/dV spectra acquired at this straight edge exhibit a pronounced peak at –50 mV (Fig. 2(b)). The intensity of the peaks at –50 mV, after subtracting the spectrum of Si/Ir as a function of position in the interior area of the GNIs (Fig. 2(c)), decays approximately exponentially as a function of the distance from the edge. In contrast, such a prominent peak can always be observed in the dI/dV spectra acquired along GNI edges (Fig. 2(d)). The dI/dV map acquired at –50 mV demonstrates that this peak is localized at the edge of the GNIs (Fig. 2(e)). This behavior indicates that the pronounced peaks at –50 mV in the dI/dV spectra can be assigned to the local electronic states arising from zigzag edges of GNIs [10, 32]. Hence, the edge states are recovered as the coupling between GNIs and the Ir substrate is sufficiently weakened by the intercalated Si layer.

The energies of edge states depend strongly on the size of the GNIs. Figure 3 illustrates the evolution of dI/dV spectra collected at zigzag edges of a selected set of GNIs with different sizes (definition of the size is shown in Fig. S5(f) in the ESM). Edge states are at –0.07 eV for the GNI with a size of about 10 nm (Fig. 3(a)). With increasing lateral size, edge states gradually shift toward the Fermi Level (E_F), and stay at the E_F for GNIs with lateral sizes > 30 nm (see Fig. 3 and Fig. S5 in the ESM). The size-dependent energy shift of edge states implies a quantum confinement of the π-electrons in the GNIs, as the quantum confinement is strongly related to the lateral size of GNIs [19, 33].

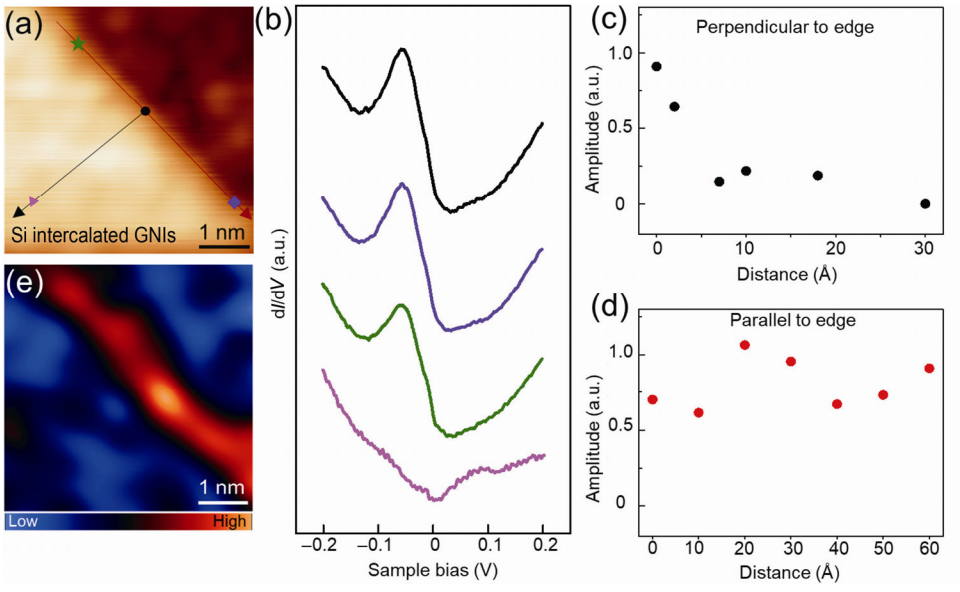

Figure 2 Edge states of Si intercalated GNIs (size is 12.9 ± 1.9 nm). (a) An STM image showing a straight edge of a Si intercalated GNI (U = –200.0 mV; I = 0.1 nA). (b) The dI/dV spectra collected at different points around the edge, marked by different dots in (a), indicating that a pronounced peak appears at –50 mV in the dI/dV spectra acquired at this straight edge. (c) The intensity of peaks at –50 mV versus distance, in a series of dI/dV spectra collected at different points along a line perpendicular to the edge (marked by the black arrow in (a)), after subtracting the dI/dV spectrum on Si/Ir(111). (d) The intensity of peaks at −50 mV versus distance, in a series of dI/dV spectra collected at different points along a line parallel to the edge (marked by the red arrow in (a)), after subtracting the dI/dV spectrum on Si/Ir(111). (e) A dI/dV map of (a) at –50 mV, showing that the edge states are spatially localized at the edge of the Si intercalated GNIs.

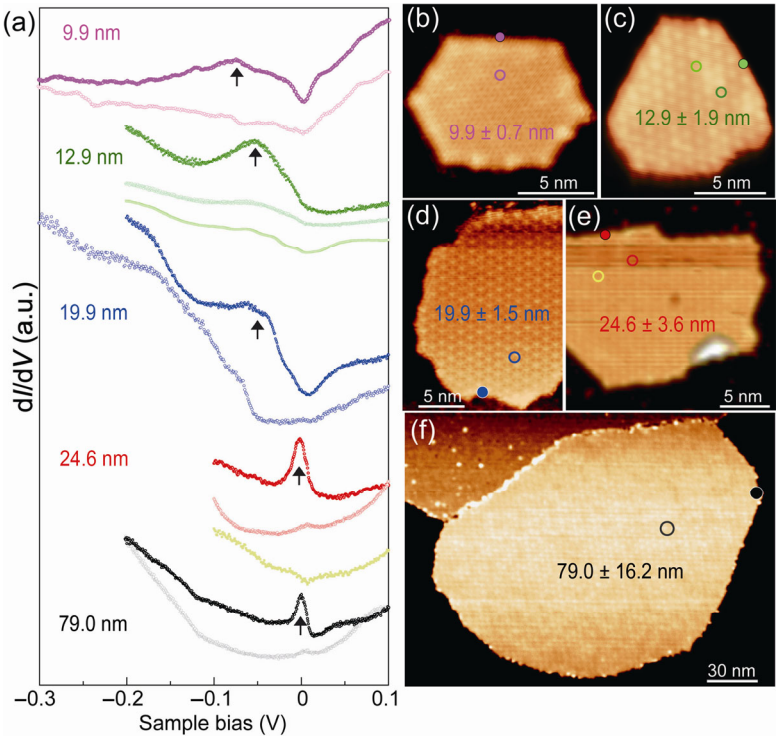

Figure 3 Size-dependent edge states of the GNIs. (a) The dI/dV spectra are collected on and far from the zigzag edges of a selected set of Si intercalated, roughly hexagonal GNIs with different lateral sizes. The curves are offset vertically with respect to their neighbors for clarity. (U = –200.0 mV, I = 0.1 nA; V_{rms} = 1.0 mV). (b)–(f) STM topographies of Si intercalated GNIs with sizes of 9.9, 12.9, 19.9, 24.6, and 79.0 nm, respectively.

In Fig. 3, the spectra of the edge sites are dominated by peaks (indicated by black arrows) that we identified as edge states. The spectra from the interior sites show weak and mostly broad peaks at different energies that have been documented in the literature and have been attributed to quantum confinement [19, 33]. The spectra in Fig. 3(a) show that the edge peaks are broader in small GNIs. The broadening is likely to arise from the fact that in the smaller GNIs the peaks move to lower energies, where there is a larger density of interior states with which they hybridize.

To confirm the recovery of the edge states of GNIs, we investigated the electronic and magnetic properties of hexagonal GNIs with various sizes by DFT calculations. As the GNIs are efficiently decoupled from the metal substrate and exhibit nearly freestanding features (see Fig. S6 in the ESM), we modeled the GNIs/Si/Ir systems as isolated freestanding GNIs without considering the metal substrate. Due to limitation by our computational capabilities, the largest GNI in the calculations has a length of eight carbon rings at each edge.

Figure 4(a) shows the calculated energy levels of hexagonal GNIs with a length from four carbon rings to eight carbon rings in each edge. By analyzing the spatial distribution of each energy level, edge states can be identified and the ones near the Fermi level are labeled with blue lines. Calculations of the GNI edge states indicate that, just as in the edges of GNRs, there are two edge states. One is occupied and lies near the Fermi energy (labeled with blue lines), as observed, while the second is at more than 1 eV above the Fermi energy and is not accessible to the experiments reported here. The behavior of the GNI edge states is different from that of GNR edge states, in that the edge states are always at the Fermi energy for GNRs. In Fig. S7 in the ESM, the distribution plot of the highest occupied molecular orbital (HOMO) in GNIs shows that, even though this state is mainly distributed in the interior, it also has a large amplitude at the edges. We found that edge states start to show up for GNIs with edge lengths larger than four carbon rings. Charge densities of these edge states are plotted

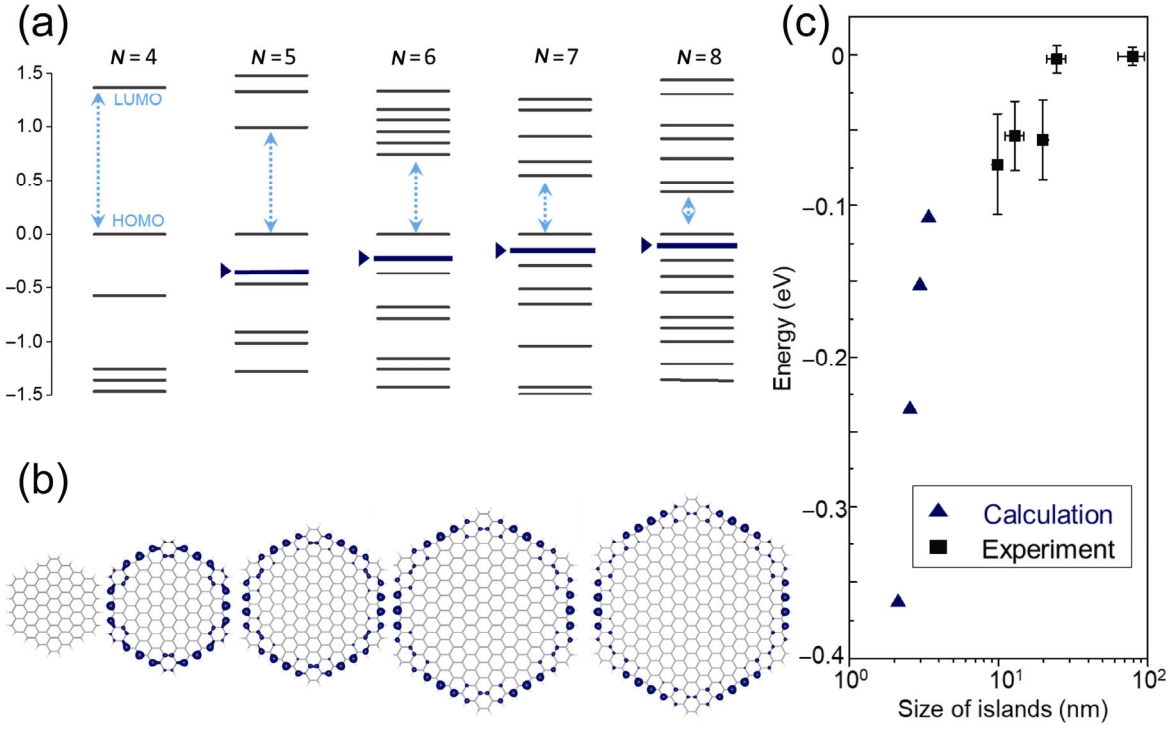

Figure 4 Positions of the edge states in GNIs of different sizes. (a) Calculated energy levels of a hexagonal GNI with a length from four carbon rings to eight carbon rings. The levels indicated by blue triangles are assigned to the edge states near the Fermi level. (b) Calculated charge density of the edge states near the Fermi level, showing their spatial localization on a hexagonal GNI with a length from four carbon rings to eight carbon rings. Edge states appear only at GNIs of lengths longer than four carbon rings. The isosurface is chosen as 0.0005 e/bohr^3. (c) The energy of the edge states versus lateral size of GNIs for both theoretical and experimental results.

in Fig. 4(b). It can be clearly seen that these states are spatially localized at the zigzag edges and thus can be assigned to the edge states of the GNIs. The spatial extension of the edge state has been checked by the dI/dV mapping in experiments. Both large island (Fig. S5(e) in the ESM) and small island (Fig. 2(e)) show a similar spatial extension of edge states (about 1.0 nm), in agreement with the results of the DFT calculations shown in Fig. 4(b). It is worth mentioning that in contrast to zigzag graphene nanoribbons (ZGNRs), in which there is ferromagnetic order at each edge, our theoretical calculations reveal that the edge states in hexagonal GNIs are not spin-polarized [4].

We also found that edge states shift upwards with an increasing lateral GNI size. GNIs with edge lengths shorter than five carbon rings have electronic structures similar to aromatic molecules and there is no edge state. Figure 4(c) plots the energy of the edge states near the Fermi level versus the lateral size of GNIs for both theoretical and experimental results. The energy of the edge states increases monotonically with increasing lateral size of GNI, as the coupling between the edge states of different edges is reduced. GNIs with a lateral size larger than 24 nm have edge states that are essentially decoupled from each other and thus become valence band maxima.

In addition to hexagonal GNIs, we also checked edge states in GNIs of different shapes (see Fig. S8 in the ESM). DFT calculations showed that when the symmetry of a hexagonal GNI decreases, GNIs become spin polarized. For the GNIs with a ribbon shape, as shown in Fig. S8(i) in the ESM, the magnetic properties are similar to those in ZGNRs; i.e. ferromagnetic order in each of the two long edges and antiferromagnetic coupling between the two opposite long edges. There is no net magnetic moment for the whole GNI. When the GNI becomes more irregular (Figs. S8(j)–S8(l) in the ESM) there is a net magnetic moment located on the long edges. This existence of polarized edge states in irregular hexagonal GNIs provides opportunities for designing graphene-based spintronic devices [6, 13].

3 Conclusions

In summary, the edge states of GNIs with zigzag edges on Ir(111) were successfully recovered by intercalating an atomic layer of Si between GNIs and Ir substrates. LT-STM/STS measurements and DFT calculations found that the intercalated Si layer acts as a buffer layer and effectively suppresses the interaction between the GNIs and Ir substrates, resulting in the recovery of edge states. The edge states gradually shifted to the Fermi level with increasing lateral sizes of the GNIs. The present work demonstrates that the edge states of graphene nanostructures can be tuned by the intercalation of foreign materials, which may be useful for the fabrication of graphene-based electronic and spintronic devices.

4 Methods

4.1 Experimental details

Experiments were carried out in an ultrahigh vacuum (base pressure of 1×10^{-10} mbar) LT-STM system (Unisoku), equipped with standard surface preparation facilities. The Ir(111) (MaTeck) surface was prepared by repeated cycles of Ar^+ sputtering and annealing at 1,150 K. GNIs were prepared by exposing clean Ir(111) to ethylene (1×10^{-6} mbar) at 300 K for 1 min and subsequent annealing at 1,100 K for 5 min. Silicon was evaporated onto the surface at 300 K and then annealed at 800 K for 20 min to realize the insertion of a Si layer at the interface of graphene/Ir. STM images were acquired in constant-current mode. All given voltages refer to the sample. Differential conductance (dI/dV) spectra were collected by using a lock-in technique with a 1 mV_{rms} sinusoidal modulation at a frequency of 973 Hz. All STM/STS experiments were performed with electrochemically etched tungsten tips at 4.2 K.

4.2 Details of the theoretical calculations

Quantum mechanical calculations based on DFT were performed using the Vienna *ab initio* simulation package (VASP) [34] and the projector augmented wave (PAW) method [35, 36]. Local density approximation (LDA) in the form of Perdew-Zunger was adopted for the exchange-correlation functional [37, 38]. The energy cutoff of the plane-wave basis set was 400 eV. Because of the periodic boundary conditions, a vacuum layer thicker than 15 Å was used to separate adjacent GNIs in order to avoid coupling between two GNIs in nei-

ghboring cells. Structural optimization was performed until the force on each atom was less than 0.01 eV/Å.

Acknowledgements

This work is supported by the National Key Research and Development Projects of China (No. 2016YFA0202300), the National Basic Research Program of China (Nos. 2013CBA01600 and 2015CB921103), the National Natural Science Foundation of China (Nos. 61390501, 51325204, 51210003, and 61622116), and the CAS Pioneer Hundred Talents Program. Work at Vanderbilt is partially supported by the Department of Energy grant DE-FG02-09ER46554 and by the McMinn Endowment. Y. Y. Z and S. T. P acknowledge the National Energy Research Scientific Computing Center (NERSC), a DOE Office of Science User Facility supported by the Office of Science of the U.S. Department of Energy under Contract No. DE-AC02-05CH11231, and the Extreme Science and Engineering Discovery Environment (XSEDE), which is supported by the National Science Foundation Grant ACI-1053575. A portion of the research was performed in CAS key laboratory of Vacuum Physics.

Electronic Supplementary Material: Supplementary material (further details of d*I*/d*V* spectra of non-intercalated GNIs, d*I*/d*V* spectra of Si-intercalated large-sized GNIs and additional DFT calculations) is available in the online version of this article at https://doi.org/10.1007/s12274-017-1940-5.

References

[1] Meunier, V.; Souza Filho, A. G.; Barros, E. B.; Dresselhaus, M. S. Physical properties of low-dimensional sp^2-based carbon nanostructures. *Rev. Mod. Phys.* **2016**, *88*, 025005.

[2] Dienel, T.; Kawai, S.; Söde, H.; Feng, X. L.; Müllen, K.; Ruffieux, P.; Fasel, R.; Gröning, O. Resolving atomic connectivity in graphene nanostructure junctions. *Nano Lett.* **2015**, *15*, 5185–5190.

[3] Joung, D.; Nemilentsau, A.; Agarwal, K.; Dai, C. H.; Liu, C.; Su, Q.; Li, J.; Low, T.; Koester, S. J.; Cho, J. H. Self-assembled three-dimensional graphene-based polyhedrons inducing volumetric light confinement. *Nano Lett.* **2017**, *17*, 1987–1994.

[4] Wang, W. L.; Meng, S.; Kaxiras, E. Graphene nanoflakes with large spin. *Nano Lett.* **2008**, *8*, 241–245.

[5] Son, Y. W.; Cohen, M. L.; Louie, S. G. Half-metallic graphene nanoribbons. *Nature* **2006**, *444*, 347–349.

[6] Cui, P.; Zhang, Q.; Zhu, H. B.; Li, X. X.; Wang, W. Y.; Li, Q. X.; Zeng, C. G.; Zhang, Z. Y. Carbon tetragons as definitive spin switches in narrow zigzag graphene nanoribbons. *Phys. Rev. Lett.* **2016**, *116*, 026802.

[7] Wimmer, M.; Adagideli, İ.; Berber, S.; Tománek, D.; Richter, K. Spin currents in rough graphene nanoribbons: Universal fluctuations and spin injection. *Phys. Rev. Lett.* **2008**, *100*, 177207.

[8] Topsakal, M.; Sevinçli, H.; Ciraci, S. Spin confinement in the superlattices of graphene ribbons. *Appl. Phys. Lett.* **2008**, *92*, 173118.

[9] Ruffieux, P.; Wang, S. Y.; Yang, B.; Sánchez-Sánchez, C.; Liu, J.; Dienel, T.; Talirz, L.; Shinde, P.; Pignedoli, C. A.; Passerone, D. et al. On-surface synthesis of graphene nanoribbons with zigzag edge topology. *Nature* **2016**, *531*, 489–492.

[10] Tao, C. G.; Jiao, L. Y.; Yazyev, O. V.; Chen, Y. C.; Feng, J. J.; Zhang, X. W.; Capaz, R. B.; Tour, J. M.; Zettl, A.; Louie, S. G. et al. Spatially resolving edge states of chiral graphene nanoribbons. *Nat. Phys.* **2011**, *7*, 616–620.

[11] Shen, J. H.; Zhu, Y. H.; Yang, X. L.; Li, C. Z. Graphene quantum dots: Emergent nanolights for bioimaging, sensors, catalysis and photovoltaic devices. *Chem. Commun.* **2012**, *48*, 3686–3699.

[12] Liu, R. L.; Wu, D. Q.; Feng, X. L.; Müllen, K. Bottom-up fabrication of photoluminescent graphene quantum dots with uniform morphology. *J. Am. Chem. Soc.* **2011**, *133*, 15221–15223.

[13] Wang, W. L.; Yazyev, O. V.; Meng, S.; Kaxiras, E. Topological frustration in graphene nanoflakes: Magnetic order and spin logic devices. *Phys. Rev. Lett.* **2009**, *102*, 157201.

[14] Fernández-Rossier, J.; Palacios, J. J. Magnetism in graphene nanoislands. *Phys. Rev. Lett.* **2007**, *99*, 177204.

[15] Heiskanen, H. P.; Manninen, M.; Akola, J. Electronic structure of triangular, hexagonal and round graphene flakes near the Fermi level. *New J. Phys.* **2008**, *10*, 103015.

[16] Yoon, Y.; Guo, J. Effect of edge roughness in graphene nanoribbon transistors. *Appl. Phys. Lett.* **2007**, *91*, 073103.

[17] Feng, X. F.; Wu, J.; Bell, A. T.; Salmeron, M. An atomic-scale view of the nucleation and growth of graphene islands on Pt surfaces. *J. Phys. Chem. C* **2015**, *119*, 7124–7129.

[18] Coraux, J.; N'Diaye, A. T.; Engler, M.; Busse, C.; Wall, D.; Buckanie, N.; Meyer zu Heringdorf, F.-J.; van Gastel, R.; Poelsema, B.; Michely, T. Growth of graphene on Ir(111). *New J. Phys.* **2009**, *11*, 023006.

[19] Phark, S. H.; Borme, J.; Vanegas, A. L.; Corbetta, M.; Sander, D.; Kirschner, J. Direct observation of electron confinement in epitaxial graphene nanoislands. *ACS Nano* **2011**, *5*, 8162–8166.

[20] Li, Y.; Subramaniam, D.; Atodiresei, N.; Lazić, P.; Caciuc, V.; Pauly, C.; Georgi, A.; Busse, C.; Liebmann, M.; Blügel, S. et al. Absence of edge states in covalently bonded zigzag edges of graphene on Ir(111). *Adv. Mater.* **2013**, *25*, 1967–1972.

[21] Lu, J.; Yeo, P. S.; Gan, C. K.; Wu, P.; Loh, K. P. Transforming C_{60} molecules into graphene quantum dots. *Nat. Nanotechnol.* **2011**,

6, 247–252.

[22] Wang, S. Y.; Talirz, L.; Pignedoli, C. A.; Feng, X. L.; Müllen, K.; Fasel, R.; Ruffieux, P. Giant edge state splitting at atomically precise graphene zigzag edges. *Nat. Commun.* **2016**, *7*, 11507.

[23] Leicht, P.; Zielke, L.; Bouvron, S.; Moroni, R.; Voloshina, E.; Hammerschmidt, L.; Dedkov, Y. S.; Fonin, M. *In situ* fabrication of quasi-free-standing epitaxial graphene nanoflakes on gold. *ACS Nano* **2014**, *8*, 3735–3742.

[24] Deniz, O.; Sánchez-Sánchez, C.; Dumslaff, T.; Feng, X. L.; Narita, A.; Müllen, K.; Kharche, N.; Meunier, V.; Fasel, R.; Ruffieux, P. Revealing the electronic structure of silicon intercalated armchair graphene nanoribbons by scanning tunneling spectroscopy. *Nano Lett.* **2017**, *17*, 2197–2203.

[25] Meng, L.; Wu, R. T.; Zhou, H. T.; Li, G.; Zhang, Y.; Li, L. F.; Wang, Y. L.; Gao, H. J. Silicon intercalation at the interface of graphene and Ir(111). *Appl. Phys. Lett.* **2012**, *100*, 083101.

[26] Mao, J. H.; Huang, L.; Pan, Y.; Gao, M.; He, J. F.; Zhou, H. T.; Guo, H. M.; Tian, Y.; Zou, Q.; Zhang, L. Z. et al. Silicon layer intercalation of centimeter-scale, epitaxially grown monolayer graphene on Ru (0001). *Appl. Phys. Lett.* **2012**, *100*, 093101.

[27] Meng, L.; Wu, R. T.; Zhang, L. Z.; Li, L. F.; Du, S. X.; Wang, Y. L.; Gao, H. J. Multi-oriented moiré superstructures of graphene on Ir(111): Experimental observations and theoretical models. *J. Phys.: Condens. Matter* **2012**, *24*, 314214.

[28] N'Diaye, A. T.; Bleikamp, S.; Feibelman, P. J.; Michely, T. Two-dimensional Ir cluster lattice on a graphene moiré on Ir(111). *Phys. Rev. Lett.* **2006**, *97*, 215501.

[29] Coraux, J.; N'Diaye, A. T.; Busse, C.; Michely, T. Structural coherency of graphene on Ir(111). *Nano Lett.* **2008**, *8*, 565–570.

[30] Jin, L.; Fu, Q.; Mu, R. T.; Tan, D. L.; Bao, X. H. Pb intercalation underneath a graphene layer on Ru(0001) and its effect on graphene oxidation. *Phys. Chem. Chem. Phys.* **2011**, *13*, 16655–16660.

[31] Kim, H. W.; Ku, J.; Ko, W.; Jeon, I.; Kwon, H.; Ryu, S.; Kahng, S. J.; Lee, S. H.; Hwang, S. W.; Suh, H. Strong interaction between graphene edge and metal revealed by scanning tunneling microscopy. *Carbon* **2014**, *78*, 190–195.

[32] Li, Y. Y.; Chen, M. X.; Weinert, M.; Li, L. Direct experimental determination of onset of electron-electron interactions in gap opening of zigzag graphene nanoribbons. *Nat. Commun.* **2014**, *5*, 4311.

[33] Hämäläinen, S. K.; Sun, Z. X.; Boneschanscher, M. P.; Uppstu, A.; Ijäs, M.; Harju, A.; Vanmaekelbergh, D.; Liljeroth, P. Quantum-confined electronic states in atomically well-defined graphene nanostructures. *Phys. Rev. Lett.* **2011**, *107*, 236803.

[34] Kresse, G.; Hafner, J. *Ab initio* molecular dynamics for liquid metals. *Phys. Rev. B* **1993**, *47*, 558–561.

[35] Kresse, G.; Furthmüller, J. Efficient iterative schemes for *ab initio* total-energy calculations using a plane-wave basis set. *Phys. Rev. B* **1996**, *54*, 11169–11186.

[36] Kresse, G.; Joubert, D. From ultrasoft pseudopotentials to the projector augmented-wave method. *Phys. Rev. B* **1999**, *59*, 1758–1775.

[37] Ceperley, D. M.; Alder, B. J. Ground state of the electron gas by a stochastic method. *Phys. Rev. Lett.* **1980**, *45*, 566–569.

[38] Perdew, J. P.; Zunger, A. Self-interaction correction to density-functional approximations for many-electron systems. *Phys. Rev. B* **1981**, *23*, 5048–5079.